

# Towards Automated Detection of Abnormalities in Lung Segmentations

Reinhard Beichel<sup>1,2,3</sup>, Simon Schlosser<sup>4</sup>, Pierre Elbischger<sup>4</sup>, Shanhui Sun<sup>1,3</sup>,  
and Geoffrey McLennan<sup>2,3</sup>

<sup>1</sup> Dept. of Electrical and Computer Engineering

<sup>2</sup> Dept. of Internal Medicine

<sup>3</sup> The Iowa Institute for Biomedical Imaging  
The University of Iowa, Iowa City, IA 52242, USA  
[reinhard-beichel@uiowa.edu](mailto:reinhard-beichel@uiowa.edu)

<sup>4</sup> Dept. of Medical Information Technology  
Carinthia University of Applied Sciences  
A-9020 Klagenfurt, Austria

**Abstract.** Automated lung segmentation in multidetector computed tomography data is a first processing step in computer-aided quantitative assessment of lung disease. Robust segmentation of diseased lungs is a non-trivial problem which is unsolved up to now. Consequently, lung segmentation results need to be manually verified, which is time-consuming and costly. We propose a novel algorithm for detecting gross abnormal lung segmentations based on a fast 3D shape retrieval approach. First, the segmentation result to verify is used to query a 3D lung shape database containing normal lung shapes. Second, the 3D shape dissimilarity between query and retrieved shape is utilized to assess the abnormality of the segmentation. Our method represents a first step toward the development of a quality assessment system for lung segmentations.

**Key words:** Segmentation abnormality detection, shape retrieval, shape context, lung segmentation

## 1 Introduction

Lung diseases like cancer, chronic obstructive pulmonary disease (COPD) or pneumonia are a major health problem. Multidetector computed tomography (MDCT) based lung imaging plays an important role in the early detection, diagnosis, and treatment of lung disease. Automated image analysis of lung MDCT data supports physicians in the quantitative assessment of lung disease [1]. One of the first steps in lung image analysis is to segment the lungs. Several approaches to lung segmentation in MDCT have been proposed. An overview can be found in [1]. The majority of approaches are based on gray-value analysis and assume that there is a large density difference between lung tissue and surrounding structures. In case of normal lungs, such approaches produce sufficiently accurate results. However, they frequently fail to deliver correct lung segmentations

if the lungs contain high density pathology regions like masses (tumors) or pneumonia. In general, the segmentation of diseased lungs is a non-trivial problem which is important for clinical applications and research.

Recently, a few papers proposing more robust lung segmentation algorithms have been published. For example, Sluimer et al. propose a segmentation by registration scheme to robustly segment diseased lungs [2, 3]. While delivering promising results, not all pathological cases could be handled successfully [3]. In addition, the proposed approach is quite computing-time intensive [3]. An adaptive border marching algorithm was presented in [4] to reliably include juxtapleural nodules in lung segmentations. An approach for the robust segmentation of lung parenchyma based on the curvature of ribs was presented in [5]. In summary, up to now available robust lung segmentation approaches are not able to handle all possible pathological cases successfully and/or require significantly more computing-time than conventional lung segmentation methods. This is especially a problem for the automated analysis of large numbers of lung MDCT data sets, as required in multi-center clinical trials or the automated processing/analysis of lung image databases collected by the Lung Image Database Consortium (LIDC) [6] or the Reference Image Database to Evaluate Response (RIDER)<sup>1</sup> projects, for example. Even the verification of the correctness of several thousand lung segmentation results is a costly and time-consuming task. To efficiently deal with this problem, an automated quality assessment/control system is needed that allows the automatic identification of abnormal lung segmentations (e.g., segmentation errors, breathing artifacts, etc.). Once abnormal segmentations are identified, different remedy strategies can be applied, including:

- adapt parameters and rerun the segmentation algorithm,
- apply a more robust—but usually more time consuming—method,
- manually correct the automatically generated segmentation result,
- switch to a semiautomatic/manual segmentation approach, or
- exclude the data set from further analysis.

A process might even utilize a sequence of the above outlined strategies depending on the classification result of the segmentation after each processing step.

In this paper we present a novel approach to detect grossly abnormal lung segmentations based on a shape retrieval method. The main idea behind our approach is as follows. First, the 3D lung segmentation result is used to query a reference lung shape database. Data sets in the reference database are representatives for normal lung shapes. Second, an assessment of the segmentation abnormality is derived from a 3D shape dissimilarity between query shape and the best match found in the reference database. Our approach builds on a fast shape retrieval approach based on shape contexts which we recently introduced for 2D shape retrieval [7]. This allows the rapid assessment of segmentation results. While content-based image retrieval systems have been developed for lung images [8, 9], we are not aware of similar approaches for 3D lung shape.

<sup>1</sup> <http://ncia.nci.nih.gov/collections>

Abnormalities in 3D shape can be caused by segmentation errors (e.g., due to high density lung pathology), breathing artifacts, pleural effusion, missing data and so on. The work described in this paper represents a first step toward the development of a lung segmentation quality assessment system that can differentiate between different causes of abnormal segmentations.

## 2 Related Work

Content-based retrieval systems are a prerequisite to effectively utilize databases like medical image archives. The two most popular query techniques in this context are semantic retrieval and query by example. In the latter case, the user provides an example depicting the content of the query. To process such a request, algorithms are needed that assess the similarity/dissimilarity between query and examples stored in a database. This allows for the ordering of the database examples based upon their relevance, and to retrieve the closest match.

Shape is an important feature for querying object databases. Several methods for 3D shape retrieval have been proposed. A review of methods can be found in [10]. In the case of large databases, the time needed to assess the similarity of images is critical for retrieval performance, and thus, for practical applicability.

Shape contexts [11, 12] represent a powerful method for shape description and similarity assessment. They have been used for applications like shape retrieval [13, 14] or hippocampal surface mapping [15]. Fig. 1 illustrates the basic idea of shape contexts on 2D shapes. Given an object in an image, a representation

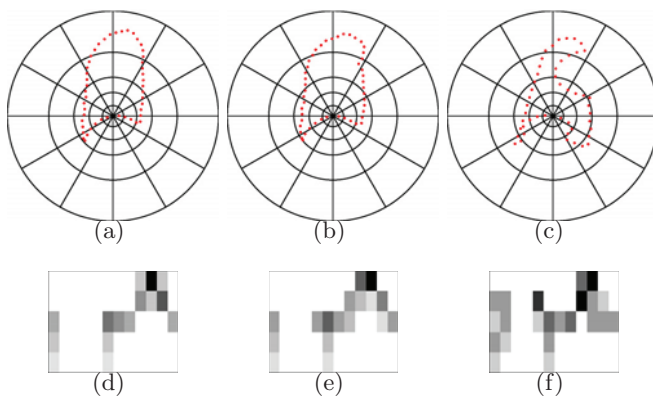


**Fig. 1.** Examples of 2D shape contexts. (a-c) Sampled object shapes shown with log-polar histogram bins placed on a reference point. (d-f) Shape contexts corresponding to (a-c).

of the object's shape based on a finite set of 2D points  $P = \{\mathbf{p}_1, \dots, \mathbf{p}_n\}$  with  $\mathbf{p}_i \in \mathbb{R}^2$  is generated by sampling the object contour. Point sampling can be

done randomly or with an equidistant spacing. A reasonable selection of  $n$ , the number of sample points, is required to have a good representation of the input shape. For a point  $\mathbf{p}_i$  of the shape represented by  $P$ , a coarse histogram  $\mathbf{H}_i$  of the relative coordinates of the remaining  $n - 1$  points is computed:

$$\mathbf{H}_i(k) = \#\{\mathbf{q} \neq \mathbf{p} | (\mathbf{q} - \mathbf{p}_i) \in \text{bin}(k)\}. \quad (1)$$

The calculated histogram  $\mathbf{H}_i$  is denoted as the shape context of  $\mathbf{p}_i$  [12]. For example, Figs. 1(a-c) depict three different 2D shapes, each with a selected reference point  $\mathbf{p}_i$  and a log-polar histogram outline around  $\mathbf{p}_i$ . The corresponding shape contexts are depicted in Fig. 1(d-f). The shape context in Figs. 1(d) and 1(e) show similarities, because the object shapes are similar (normal lung shapes) and reference points on both of the shapes have been chosen such that they are approximately corresponding. In contrast, the similarities of the shape contexts of the normal lung shapes (Figs. 1(d-e)) and the abnormal lung shape (Fig. 1(f)) are quite low. Consequently, shape contexts can be utilized to compare shapes.

The bins of the histogram are usually chosen such that they are uniform in log-polar space, which makes the descriptor more sensitive to shape points nearby the point  $\mathbf{p}_i$ . Normalization to rotation of a shape is achieved by aligning the histogram with the shape tangent or normal vector direction in point  $\mathbf{p}_i$ . Invariance to isotropic scaling can be gained by normalizing the shapes regarding their size before they are used to calculate the shape context.

For shape retrieval, the similarity/dissimilarity between the query shape and all the shapes in a database need to be assessed. For example, this can be accomplished by using shape contexts. As outlined in [7], a major drawback of utilizing shape contexts directly for shape retrieval is the high computing-time needed for the comparison of a query shape with shapes in a database, since each shape is usually described by several hundred or thousand shape contexts which need to be compared individually. Consequently, methods that utilize a single shape signature are preferable for shape retrieval, especially when large databases are queried.

### 3 Method

Our approach to detect gross abnormalities in lung segmentations consists of two main processing steps. First, the given lung segmentation is used to query a 3D lung shape database containing normal lung shapes. Second, the 3D shape dissimilarity between retrieval result and query segmentation is used to assess the segmentation. The left and right lung are processed independently, thus we utilize two databases of normal left and right lung shapes. However, the processing scheme is the same for left and right lungs. The individual components of our method are described in detail in the following sections.

#### 3.1 Fast 3D Shape Retrieval

For efficient 3D shape retrieval from a database, we use a shape signature which is based on shape contexts. The utilized approach represents an extension of

our previous work on fast 2D shape retrieval [7] to 3D. The main idea behind our approach is outlined in Fig. 3. For a given 3D shape, represented by a point set  $P = \{\mathbf{p}_1, \dots, \mathbf{p}_o\}$  with  $\mathbf{p}_i \in \mathbb{R}^3$  (Figs. 3(a-c)), all the corresponding shape histograms  $\mathbf{H}_i$  with  $i = 1, \dots, o$  are calculated. The 3D (spherical) shape contexts  $\mathbf{H}_i$  (Fig. 2) are then rearranged into 1D shape context vectors  $\mathbf{v}_i$ , based on which a single shape signature is calculated for  $P$  (Figs. 3(d-f)). The similarity of two shapes can then be assessed by comparing the corresponding shape signatures. Basically, the task of assessing shape similarity is transformed into the task of assessing the similarity of shape signatures. Consequently, in terms of computing time, expensive point-to-point shape context comparisons are avoided.

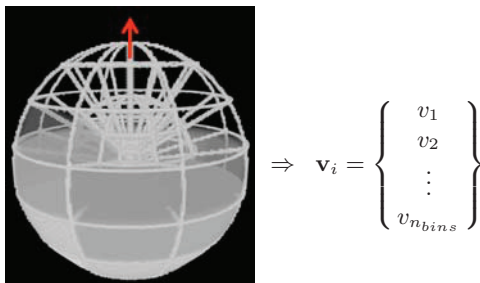


**Fig. 2.** Example of a 3D (spherical) shape context histogram  $\mathbf{H}_i$  and the corresponding rearranged shape context vector  $\mathbf{v}_i$ . A log-polar partitioning scheme is used to define the 3D histogram bins. To gain invariance to rotation, the axis of the shape histogram (red arrow) is aligned with the surface normal at a sample point  $\mathbf{p}_i$ . The bin content is rendered in gray.

Given two 3D point sets  $P_x = \{\mathbf{p}_{x,1}, \dots, \mathbf{p}_{x,m}\}$  and  $P_y = \{\mathbf{p}_{y,1}, \dots, \mathbf{p}_{y,n}\}$  to compare, let the matrices  $\mathbf{S}_x = [\mathbf{v}_{x,1}, \dots, \mathbf{v}_{x,m}]^T$  and  $\mathbf{S}_y = [\mathbf{v}_{y,1}, \dots, \mathbf{v}_{y,n}]^T$  store all the rearranged shape context vectors of the shapes  $P_x$  and  $P_y$ , respectively. We then define the following shape dissimilarity measure:

$$SD(P_x, P_y) = 1 - \text{corr}(\text{scc}(P_x), \text{scc}(P_y)), \quad (2)$$

where the shape context covariance (signature) of a point set  $P$  is defined as  $\text{scc}(P) = \text{cov}(\mathbf{S})$ , and  $\text{cov}(\mathbf{S})$  denotes the covariance matrix of all the rows (shape context vectors) in  $\mathbf{S}$ . The function  $\text{corr}$  in Eq. 2 denotes the normalized correlation coefficient. Low values for  $SD$  indicate a high similarity, and large values indicate shapes with low similarity. Given a query shape  $P_{\text{query}}$  and a normal lung shape database  $DB = \{P_1, \dots, P_w\}$ , the shape retrieval result  $P_{i_{\text{match}}}$  is generated by evaluating  $i_{\text{match}} = \arg \min_{i=1, \dots, w} \{SD(P_{\text{query}}, P_i)\}$  with  $P_i \in DB$ . To speedup the retrieval process, all shape signatures  $\text{scc}(P_i)$  of database shapes can be calculated in an offline processing step and stored in the database. In addition, only the upper triangular part of  $\text{scc}(P)$  needs to be

considered for correlation calculation and storage, because of the symmetry of the covariance matrix. This reduces computing-time and the required storage space for the shape signatures. Matrices  $\mathbf{S}_x$  and  $\mathbf{S}_y$  are of size  $m \times n_{bins}$  and  $n \times n_{bins}$ , respectively.  $n_{bins}$  denotes the number of histogram bins. The numbers  $m$  and  $n$  of points in each point set can be different, but we prefer that  $m$  and  $n$  are the same. Consequently, we randomly sample  $u = m = n$  points from the surface of the left and right segmented lung shape.

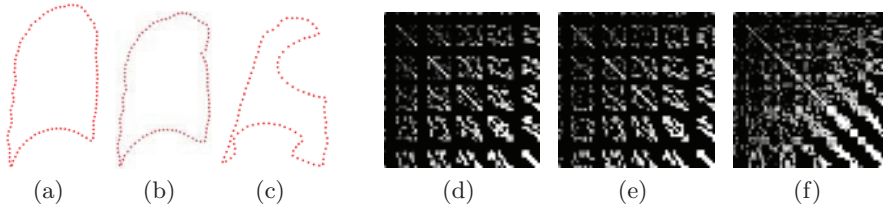


**Fig. 3.** 2D example of shape signatures derived from shape contexts. (a-c) Point sets representing shapes. (d-f) Corresponding shape signatures  $\mathbf{H}$ ; a nonlinear gray-value transformation was applied for better visualization of signature patterns.

To gain invariance to rotation, a surface normal vector is calculated for each sample point (Fig. 4(e)) to align the shape context. To robustly compensate for differences in size, we utilize the following approach. The left and right lungs of the database are roughly normalized before the shape signature is calculated by isotropically scaling them so that they have a height of  $h_l = 260$  mm (approx. average lung size in  $z$ -direction). To calculate shape contexts of database shapes, a minimum radius of  $r_{min_{DB}} = 6$  mm and maximum radius of  $r_{max_{DB}} = h_l/3$  is used. Furthermore, after sampling shape points from the query data set, several shape signatures  $scc(P_{query}, \gamma) = scc_\gamma(P_{query})$  are calculated by using  $r_{min_{Q\gamma}} = \gamma r_{min_{DB}}$  and  $r_{max_{Q\gamma}} = \gamma r_{max_{DB}}$  with the scale factor  $\gamma \in O$  and  $O = \{0.5, 0.6, \dots, 1.5\}$  for the log-polar histograms. The size invariant shape retrieval match  $P_{i_{match\_SI}}$  is found by evaluating

$$i_{match\_SI} = \arg \min_{i=1, \dots, w} \{SD(P_{query}, \gamma_i, P_i)\} \quad (3)$$

with  $\gamma_i = \arg \min_{\gamma \in O} \{SD(P_{query}, \gamma, P_i)\}$ . The corresponding parameter  $\gamma_{i_{match\_SI}}$  represents a discrete estimate for the relative size between query shape and retrieved normalized shape from the lung database.

Depending on the imaging protocol used, the scans can show heart motion artifacts. In addition, ribs, airways, as well as pulmonary arteries and veins can cause certain local variations in shape (Figs. 4(a) and (b)). To better deal with this variation, we smooth the volumetric lung shape data sets by applying a convolution with a Gaussian kernel ( $\sigma = 10$ ) before the surface points are sampled. Examples for smoothed lung shapes are shown in Figs. 4(c) and (d). In comparison, the corresponding original shapes are shown in Figs. 4(a) and (b).

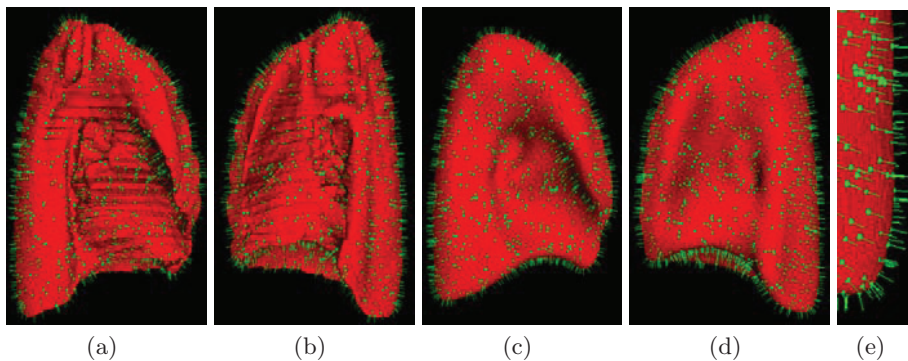


**Fig. 4.** Sampled surface points utilized to describe lung shapes shown with corresponding normal vectors. (a) Left and (b) right lung. (c) Smoothed lung shape corresponding to (a). (d) Smoothed lung shape corresponding to (b). (e) Magnified lower right section of the smoothed lung shown in (d).

Let  $SD_{DB}(P_{query})$  denote the dissimilarity between query and retrieved database shape. Gross shape abnormalities can be detected by applying a threshold to  $SD_{DB}(P_{query})$ .

## 4 Experiments

For our experiments, we utilized 54 left and 57 right lung shapes for building a normal lung shape database. In addition, 22 left and 16 right gross abnormal lung segmentations were available. Abnormalities were caused by different kinds of lung pathology (e.g., cancer), missing data, segmentation errors, and severe breathing artifacts. All lung shapes were represented by  $u = 4000$  randomly selected surface sample points. The selection of  $u$  represents a good trade-off between computing time, needed for calculating shape histograms, and the ability to describe local surface details. Shape histograms with  $n_{bins} = 360$  were utilized (partitioning scheme: 5, 8, and 9 bins for radius, longitude, and latitude, respectively; see Fig. 2).

Two experiments were performed to assess our method. First, we performed a leave-one-out experiment on the database shapes. There are two reasons behind this experiment. First, the experiment allows us to find out how well the left out shape is represented in the database. This is an important analysis, because we have a limited number of database shapes for the left and right lung. Clearly, the more lung shape cases are stored in the database, the better the population can be described. Second, it allows us to find out which 3D shape dissimilarity ( $SD$ ) values we can expect for normal lung shapes. In the second experiment, the available abnormal left and right lung shapes were used to query the corresponding normal lung shape databases. The  $SD$  histograms of both experiments are plotted in Figs. 5(a) and (b) for the left and right lung, respectively. And the corresponding receiver operating characteristics (ROC) are shown in Fig. 6.

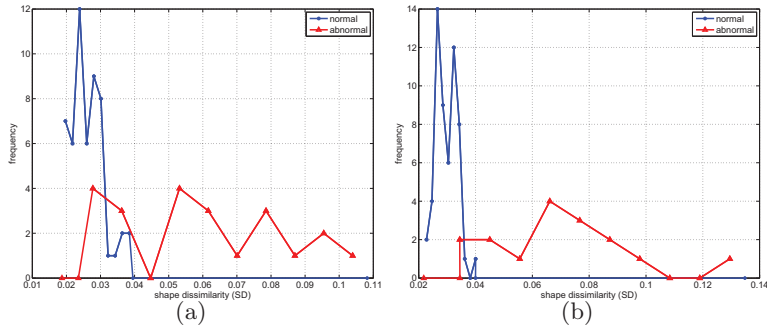


**Fig. 5.** Shape dissimilarity ( $SD$ ) histograms for normal and gross abnormal shapes. (a) Left lung and (b) right lung.

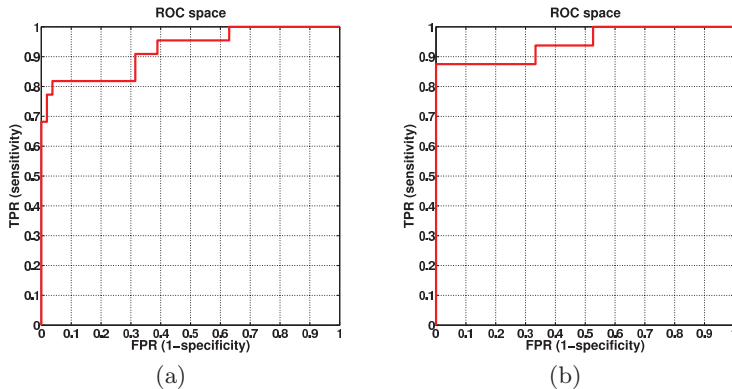


**Fig. 6.** Receiver operating characteristics (ROC) for the (a) left and (b) right lung.

The time required for producing a point representation of a query segmentation was 220 seconds. The generation of the eleven shape signatures needed for gaining size invariance took 72 seconds. The intrinsic shape retrieval process required 0.5 seconds on average. Our experiments were performed on a standard image pressing workstation, and the utilized implementation was not optimized for speed.

## 5 Discussion

The shape dissimilarity ( $SD$ ) histograms in Figs. 5 show that normal lung shapes have quite low  $SD$  values compared to abnormal shapes. For the left and right lung shapes, there is some overlap in terms of shape dissimilarity. This is also clearly visible in the ROC plots in Fig. 6. One cause for this might be that some normal shapes are not well represented in our database. For the reported experiments, a limited number of lung shapes was available. Clearly, the currently

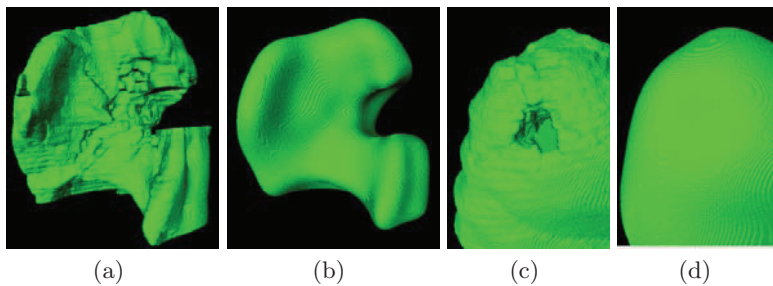


**Fig. 7.** Impact of surface smoothing. (a) and (c) Lung segmentations containing segmentation errors; (b) and (d) corresponding smoothed lung shapes. The gross segmentation error is clearly visible in (b), but the error caused by a tumor in (c) is not visible in (d) due to size.

utilized number of database shapes is not representative for all possible lung shapes, as indicated by our experiments. For example, barrel chest “shaped” lungs are underrepresented. In this context, we plan to evaluate our method on a larger data collection in the future.

Using smoothed lung shapes for analysis clearly represents a trade-off. On the one hand, only basic shape characteristics are utilized for shape analysis, and heart motion artifacts, rib patterns on the lung surface, etc. do not influence the shape dissimilarity measure. On the other hand, some (smaller) abnormalities might not be detected, because they are not or only allusively represented by the smoothed shape (Fig. 7). In this paper, we are specifically aiming at assessing/detecting gross abnormalities based on shape analysis. In the future we plan to expand our approach by utilizing shape representations on different scales. This will allow us to detect more and smaller abnormalities. In this context, calculating shape signatures for specific sub-parts of lung shapes might also enable to detect smaller and local abnormalities.

## 6 Conclusion

We have presented an approach to assess grossly abnormal lung segmentations based on a shape retrieval approach. Our method represents a step towards the development of an automated quality assessment system. Such a system will be beneficial for the automated analysis of large numbers of MDCT lung scans. In addition, it offers the prospect of developing novel approaches to robust lung segmentation.

## 7 Acknowledgments

The authors thank Sudharshan Reddy Bommur and Joseph Reinhardt at The University of Iowa for providing segmented lung data sets. This work was supported in part by the Austrian Marshall Plan Foundation.

## References

1. Sluimer, I., Schilham, A., Prokop, M., van Ginneken, B.: Computer analysis of computed tomography scans of the lung: a survey. *IEEE Trans. Med. Imag.* **25**(4) (2006) 385–405
2. Sluimer, I.C., Niemeijer, M., van Ginneken, B.: Lung field segmentation from thin-slice CT scans in presence of severe pathology. In: *Proc. SPIE (Medical Imaging)*. Volume 5370. (2004) 1447–1455
3. Sluimer, I., Prokop, M., van Ginneken, B.: Toward automated segmentation of the pathological lung in CT. *IEEE Trans. Med. Imag.* **24**(8) (2005) 1025–1038
4. Pu, J., Roos, J., Yi, C.A., Napel, S., Rubin, G.D., Paik, D.S.: Adaptive border marching algorithm: Automatic lung segmentation on chest CT images. *Computerized Medical Imaging and Graphics* **32**(6) (2008) 452 – 462
5. Prasad, M.N., Brown, M.S., Ahmad, S., Abtin, F., Allen, J., da Costa, I., Kim, H.J., McNitt-Gray, M.F., Goldin, J.G.: Automatic segmentation of lung parenchyma in the presence of diseases based on curvature of ribs. *Academic Radiology* **15**(9) (2008) 1173 – 1180
6. Meyer, C.R., Johnson, T.D., McLennan, G., Aberle, D.R., Kazerooni, E.A., Macmahon, H., Mullan, B.F., Yankelevitz, D.F., van Beek, E.J.R., Armato, S.G., McNitt-Gray, M.F., Reeves, A.P., Gur, D., Henschke, C.I., Hoffman, E.A., Bland, P.H., Laderach, G., Pais, R., Qing, D., Piker, C., Guo, J., Starkey, A., Max, D., Croft, B.Y., Clarke, L.P.: Evaluation of lung MDCT nodule annotation across radiologists and methods. *Acad Radiol* **13**(10) (Oct 2006) 1254–1265
7. Schlosser, S., Beichel, R.: Fast shape retrieval based on shape contexts. In: *Proceedings of the 6th International Symposium on Image and Signal Processing and Analysis (ISPA)*, Salzburg, Austria (September 2009) in print.
8. Dy, J.G., Brodley, C.E., Kak, A., Broderick, L.S., Aisen, A.M.: Unsupervised feature selection applied to content-based retrieval of lung images. *IEEE Trans. Pattern Anal. Mach. Intell.* **25**(3) (2003) 373–378
9. Aisen, A.M., Broderick, L.S., Winer-Muram, H., Brodley, C.E., Kak, A.C., Pavlopoulou, C., Dy, J., Shyu, C.R., Marchiori, A.: Automated Storage and Retrieval of Thin-Section CT Images to Assist Diagnosis: System Description and Preliminary Assessment. *Radiology* **228**(1) (2003) 265–270
10. Tangelder, J.W.H., Veltkamp, R.C.: A survey of content based 3D shape retrieval methods. *Journal Multimedia Tools and Applications* **39**(3) (2008) 441–471
11. Belongie, S., Malik, J.: Matching with shape contexts. In: *Proc. IEEE Workshop on Content-based Access of Image and Video Libraries*. (2000) 20–26
12. Belongie, S., Malik, J., Puzicha, J.: Shape matching and object recognition using shape contexts. *IEEE Transactions on Pattern Analysis and Machine Intelligence* **24** (2002) 509–522
13. Daliri, M.R., Torre, V.: Robust symbolic representation for shape recognition and retrieval. *Pattern Recogn.* **41**(5) (2008) 1782–1798
14. Leibe, B., Schiele, B.: Analyzing appearance and contour based methods for object categorization. In: *Proc. IEEE Computer Society Conference on Computer Vision and Pattern Recognition*. Volume 2. (2003) 409–415
15. Shi, Y., Thompson, P.M., de Zubicaray, G.I., Rose, S.E., Tu, Z., Dinov, I., Toga, A.W.: Direct mapping of hippocampal surfaces with intrinsic shape context. *NeuroImage* **37**(3) (2007) 792–807